Ab-initio Study of Oxygen Vacancy Stability in Bulk and Cerium-doped Lutetium Oxyorthosilicate

Yongchao Jia[a,*], Anna Miglio[a], Xavier Gonze[a], Masayoshi Mikami[b]

[a] *European Theoretical Spectroscopy Facility, Institute of Condensed Matter and Nanosciences, Université catholique de Louvain, Chemin des étoiles 8, bte L07.03.01, B-1348 Louvain-la-Neuve, Belgium*
[b] *Functional Materials Design Laboratory, Yokohama R&D Center, Mitsubishi Chemical Corporation, 1000, Kamoshida-cho Aoba-ku, Yokohama, 227-8502, Japan*

Abstract

We study from first principles the stability of neutral and charged oxygen vacancies in lutetium oxyorthosilicate, Lu_2SiO_5, as well as its possible modification due to the presence of Ce^{3+}, as present in commercial scintillators. We show that the neutral oxygen vacancy with the lowest formation energy forms at the oxygen sites within the [SiO_4] tetrahedra instead of the interstitial oxygen site bonded exclusively to lutetium atoms. The discrepancy with a previous study is attributed to the quality of the pseudopotential. Support for these results is found by performing a bonding analysis of the oxygen sites, as well as oxygen vacancy calculations in the iso-structural Y_2SiO_5 compound. In addition, we find that the incorporation of Ce^{3+} ion does not affect the stability of oxygen vacancies in Lu_2SiO_5.

Keywords: Scintillator, Oxygen vacancy, Luminescence, Ab-initio calculation

*Corresponding author
Email address: yongchao.jia@uclouvain.be (Yongchao Jia)

1. Introduction

Since the 1990s, many efforts have been devoted to the study of the luminescent properties of Ce^{3+}-doped Lu_2SiO_5 (LSO) due to its superior characteristics for scintillation, such as a high density (7.4 g/cm^3), short decay time (around 40 ns), high light output (3.5 times that of bismuth germanate [BGO]), and a satisfactory energy resolution. [1, 2, 3, 4, 5, 6] These properties make this optical material a suitable commercial scintillator for applications in positron emission tomography (PET) imaging system.

LSO crystallizes in a monoclinic crystal structure (space group of C2/c) and its conventional cell (with 64 atoms) is shown in Figure 1, which is two times larger of the unit cell (with 32 atoms). In this compound there are five kinds of oxygen sites coordinated by Si and Lu atoms. LSO has two inequivalent Lu crystallographic sites, coordinated by seven and six oxygen atoms and denoted as Lu1 and Lu2, respectively.

When doped, the Ce ions are expected to occupy the Lu sites, as Ce and Lu have the same formal valence charge and similar ionic radii.[7] In a pioneering work on LSO:Ce^{3+}, Suzuki and co-workers measured the excitation and emission spectra of this scintillator at 11K.[2] Their results clearly indicated the presence of two distinct types of luminescent centers in LSO:Ce^{3+}. The emission band with higher energy has a peak at 420 nm and the emission band with lower energy has its maximum at 480 nm. In subsequent studies, much attention has been paid to understand the optical behavior of Ce^{3+} ion in LSO,[4, 5, 6, 8, 9, 10, 11] leading to several achievements, such as increase of light yield, higher energy resolution and shorter decay time.

However, to further understand the LSO:Ce^{3+} behavior, there are still open issues to address. Let us mention some of them. (i) The identification of the luminescent center is not yet clear and the related thermal quenching behavior lacks understanding.[12, 13] The lower emission band observed in the experiment at low temperature 11 K does not allow to identify the typical doublet emission peaks ($^2F_{7/2}$ and $^2F_{5/2}$) of Ce^{3+} ion. Furthermore, this emission band suf-

fers from a very strong thermal quenching, and it cannot be detected at room temperature.[2] In the literature there are indeed some works devoted to the identification of the luminescent center of the low emission peak.[9, 14] However, a solid assessment is still missing from those previous studies. (ii) The physical origin of the afterglow and thermoluminescence (TL) phenomenon is still controversial.[6, 8, 10, 15, 16] The afterglow and TL behaviors of LSO:Ce^{3+} degrade its scintillation properties. The main hypothesis is the presence of intrinsic defects (oxygen vacancies) created during the synthesis process of LSO:Ce^{3+} in oxygen poor atmosphere (Ar). These intrinsic defects can provide electron and/or hole traps for the excitation energy. (iii) The effect of co-doping with divalent cation ion (M^{2+}) on the scintillating performance of LSO:Ce^{3+} is not yet understood. Several recent experimental works indicate that the scintillating performance of LSO:Ce^{3+} can be improved through the co-doping of divalent cation ions.[17, 18] In these works, the improvement has been linked to the formation of intrinsic defects in LSO:Ce^{3+}. Further studies need to be conducted to confirm this hypothesis.

On the basis of the problems and hypotheses mentioned above, many experimental works have been conducted to study the intrinsic defects in LSO, especially oxygen vacancies due to oxygen-poor conditions in the synthesis process. In this respect, a pioneering study of Dorenbos'group aimed at explaining the afterglow and TL behaviors of Ce^{3+} ions luminescence.[8] Later, Cooke *et al* studied the intrinsic afterglow and TL behavior in LSO and YSO (Y_2SiO_5, iso-structural with Lu_2SiO_5) crystals and obtained a similar result for both materials.[10] Very recently, electron spin resonance (EPR) measurements were used to study the role of oxygen vacancies as electron and hole traps in YSO.[6]

Theoretical studies were also conducted to understand the stability of oxygen vacancy in orthosilicates.[15, 16] Detailed work on LSO by Liu *et al*[15] leads to the conclusion that the most stable oxygen vacancies (neutral and doubly positive charged) are created in the interstitial oxygen sites bonded to Lu atoms only. On the other hand, the result of a related study that focused on the oxygen vacancies in YSO[16] indicated that the neutral oxygen vacancies

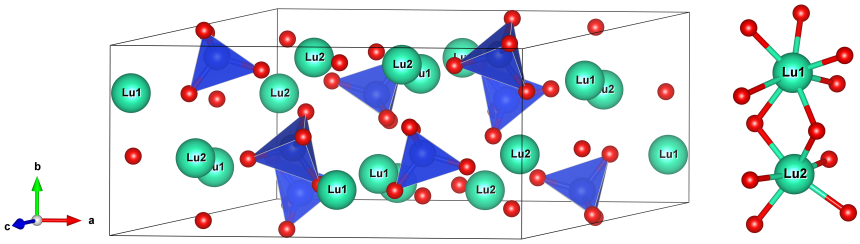

Figure 1: Crystal structure of Lu_2SiO_5 and the coordination environment of Lu sites. Green, blue and red spheres stand for Lu, Si and O atoms, respectively.

located within [SiO_4] tetrahedra are the most stable ones. As a consequence, the identification and stability of oxygen vacancies in rare-earth oxyorthosilicates with C2/c space group needs to be further examined, and the difference explained, if it is confirmed.

Although in the long term we focus on understanding the Ce^{3+} ions luminescence in LSO from first principles, which includes estimating the effect of intrinsic defects (oxygen vacancy) on the Ce^{3+} ions, it is mandatory to clarify the stability of oxygen vacancies and to provide the basis for further studies related to the neutral excitation of Ce^{3+} ion.

The present work is structured as follows. In Section 2, we first describe the theoretical methods used in the oxygen vacancy calculations. In Section 3, the structural and electron properties of LSO bulk are discussed. The stability of oxygen vacancies is studied in the Section 4, and the obtained results are validated with those from calculations on YSO and a local orbital bonding analysis. The effect of Ce^{3+} ion doping on the stability of the oxygen vacancies is illustrated in Section 5.

2. Numerical approach

2.1. General Computational Details

Calculations were performed within density functional theory (DFT) using both the norm-conserving pseudopotential and the projector augmented wave (PAW) methods as implemented in the ABINIT package.[19, 20, 21, 22] The exchange-correlation (XC) effect on the stability of oxygen vacancies in LSO (and YSO) was examined using both the LDA and the PBE-GGA. Specifically, we considered four cases: the PBE-GGA XC functional associated with a recent PAW dataset [23, 24]; the LDA XC functional, with three different norm-conserving pseudopotential sets. The first set, denoted LDA-TM, was generated about twenty year ago using the Troullier-Martins (TM) construct [25]. The second, denoted LDA-FHI, set used also the TM construct, but different (more recent) settings as implemented in the Fhi98PP pseudopotential program[26]. The third set, based on the ONCVPSP construct, was recently produced in the framework of the PseudoDojo project.[27, 28] Here we denoted it as LDA-Dojo. Most of the atomic datasets are available from the ABINIT website.

The calculation with the PBE-PAW approach is the workhorse of our LSO study. The other (LDA) cases aim at understanding the discrepancy with the earlier study, and aim at confirming the result obtained in the PBE-PAW case. For the Ce^{3+} doped calculation, DFT(PBE)+U was used, allowing the Ce_{4f} states to be found inside the band gap. The U value has been optimized to 4.6 eV (J = 0.5 eV) in our previous study on Ce^{3+} doped materials,[29], and we have not changed this value.

For the PBE-PAW case, the oxygen dataset, with $2s^2 2p^4$ valence electrons, has a 1.3 Bohr radius and two projectors per angular momentum channel. The silicon PAW dataset, with $3s^2 3p^2$ valence electrons, has a 1.71 Bohr sphere radius and two projectors per angular momentum channel. The cerium dataset, with $5s^2 5p^6 6s^2 5d^1 4f^1$ valence electrons, has a 2.5 Bohr radius and two projectors per angular momentum channel. For Lu, we tested two different PAW

atomic datasets in our previous study.[29] The normal ABINIT Lu PAW dataset, with $5s^2 5p^6 6s^2 5d^1 4f^{14}$ as valence electrons, has a 2.5 Bohr sphere radius and two projectors per angular channel. However, we assumed that Lu_{4f} electrons play a minor role on structure relaxation and electronic structure. In order to decrease the computational load in this work, we have generated a PAW atomic dataset with the valence configuration $5s^2 5p^6 6s^2 5d^1$ (freezing the fully occupied $4f$ orbital in the core state), using the ATOMPAW software[30] with the same input parameter as the normal PBE-PAW atomic dataset, but with frozen $4f$ states. Here we denote this PAW atomic dataset as 'Lu_{4f}-core', which is used in this work.

With the above PBE atomic datasets, as well as the ones from the three sets of LDA norm-conserving pseudopotentials, we performed the structural relaxation and band structure calculations. The convergence criteria have been set to 10^{-5} Hartree/Bohr (for residual forces) and 0.5 mHa/atom (for the tolerance on the total energy). In the calculations, the needed cutoff kinetic energy and Monkhorst-Pack sampling have been determined to be 30 Ha and 2×4×4, respectively.

In our work, we have also analyzed the local bonding interaction in LSO, to aid the understanding of relative stability of five kinds of oxygen vacancies. This was done using the COHP framework as implemented in the LOBSTER software.[31, 32, 33]

2.2. Defect calculations

The formation energy of oxygen vacancies (with neutral, one positive and doubly positive charged) in both LSO and YSO has been calculated using a well-established thermodynamic formalism:[34]

$$\Delta E_{\mathrm{f}}(q) = E_{\mathrm{def}}(q) - E_{\mathrm{bulk}} + q(\epsilon_{\mathrm{VBM}} + \mu_{\mathrm{e}}) - \sum_{\mathrm{i}} \Delta n_{\mathrm{i}} \mu_{\mathrm{i}} \qquad (1)$$

where E_f is the formation energy of the oxygen vacancy in a charge state q which is 0, 1+, 2+ for V_O, V_O^+ and V_O^{2+}, respectively. $E_{def}(q)$ is the total energy

of the system containing the oxygen vacancy in a charge state q and E_{bulk} is the total energy of the ideal host with the same supercell size. The third term in Eq.(1) describes the dependence on the electron chemical potential, μ_e, which is measured with respect to the valence band maximum (VBM), ϵ_{VBM}. The formation energy also depends on the chemical potential of the constituents as given by the last term, where the difference between the number of atoms of type i in the ideal cell with respect to the defect cell, is denoted by Δn_i. In the calculations, the chemical potential of oxygen, μ_O was obtained from the total energy of an O_2 molecule in a cubic box of 30×30×30 $Å^3$. In the present work, we focus on the relative stability of various oxygen vacancies in LSO(:Ce). Thus, the reference chemical potential, μ_O from the O_2 molecule is used, which might be different from the real case in oxygen poor conditions. Following above ideas, for example the formation energy of neutral oxygen vacancy in LSO without ($\Delta E_{f,1}$) and with ($\Delta E_{f,2}$) Ce^{3+} ion doping can be expressed as follows:

$$\Delta E_{f,1} = E_{tot}(LSO : V_O) + \mu_O - E_{tot}(LSO) \tag{2}$$

$$\Delta E_{f,2} = E_{tot}(LSO : Ce, V_O) + \mu_O - E_{tot}(LSO : Ce) \tag{3}$$

Furthermore, the defect thermodynamic transition energy level $\varepsilon(q/q')$ of the oxygen vacancy then can be defined as the electron chemical potential where the formation energy of oxygen vacancy in the charge state q is equal to the one of another charge state q' of the same oxygen vacancy site:[34]

$$\varepsilon(q/q') = [\Delta E_f(q) - \Delta E_f(q')]/(q' - q) \tag{4}$$

For the charged oxygen vacancy (1+ and 2+) case, additional attention must be paid to the unphysical electrostatic interaction between the charged defect and its periodic images introduced by the periodic boundary conditions. Well-established formalisms exist to correct for this artificial interaction. In the present work, we consider corrections for the dominant contribution related to

the Madelung energy:[35]

$$E^{\mathrm{Md}} = -\frac{\alpha q^2}{2\varepsilon L} \tag{5}$$

where q denotes the charge state of oxygen vacancy, α is the lattice-type dependent Madelung constant, ε is the macroscopic dielectric constant and L is the supercell lattice constant. The monopole correction term, $-\frac{\alpha q^2}{2L}$, is obtained from our ab-initio calculations, and the experimental values of the dielectric constants of LSO and YSO 9.59 and 9.94, respectively, are used.[36]

Detailed convergence studies have been conducted on the supercell size used for the oxygen vacancy calculations. For the bulk sample, the formation energies of oxygen vacancies from a 63-atom supercell differ from those of a 127-atom supercell (1×2×1 conventional cell) by less than 0.05 eV. After the Ce^{3+} ion doped, the formation energies of oxygen vacancies from a 63-atom supercell provide a slightly larger difference from those of a 127-atom supercell, around 0.1 eV. Therefore, the data presented in the main text were obtained using a 63-atom supercell for the bulk sample, which is the choice done in Ref.[15], for fair comparison. For the Ce^{3+} ion doped LSO, we use the supercell size of 127-atom. In detail, for the calculation of oxygen vacancies in LSO bulk, one oxygen atom was removed from the 64-atom LSO conventional supercell, resulting in $\mathbf{Lu_{16}Si_8O_{39}}$ **(63-atom supercell)**. The calculations involving the Ce^{3+} ion were performed with one Ce atom substituting one Lu atom both in the bulk supercell ($Lu_{32}Si_{16}O_{80}$) and in the supercell containing an oxygen vacancy ($\mathbf{Lu_{32}Si_{16}O_{79}}$**, 127-atom supercell**).

3. Bulk Lutetium Oxyorthosilicate

The structural parameters used to build the initial conventional cell were taken from experimental data [37] and then optimized in each case for the specific XC functional and pseudopotential. Table 1 lists the optimized lattice parameters for LSO obtained from PBE-PAW calculation. The theoretical results for LSO bulk are consistent with the experimental value, within 2% relative difference. The relaxation results from other three LDA calculations are also

listed in Table S1 of the Supplementary Information. The LDA-FHI and LDA-Dojo provide the optimized lattice parameters within 2% relative difference with respect to experiment, while the results of the LDA-TM case give a larger error, above 5%. At present, the larger error of LDA-TM case is not clear, but should be related to the quality of pseudopotential set, which was generated twenty years ago.

Table 1: Lattice parameters of bulk LSO within the conventional cell.

LSO	a(Å)	b(Å)	c(Å)	α	β	γ	Volume(Å^3)
Exp.	14.28	6.64	10.25	90.00	122.22	90.00	821.74
Cal.(PBE)	14.26	6.67	10.30	90.00	121.97	90.00	831.49

Figure 1 shows the optimized crystal structure. LSO is composed of edge-sharing [LuO_7] and [LuO_6] polyhedra that form a dense network with large voids accommodating the [SiO_4] tetrahedra. The relaxed coordination polyhedra of Lu^{3+} ions in this compound are also shown in Figure 1. There are indeed two inequivalent Lu sites and one Si crystal site in the LSO, which are coordinated by oxygen atoms. Five kinds of oxygen atom sites are present in the LSO structure. Figure 2 depicts the local environments of these oxygen sites. In Table 2, the five different oxygen sites are listed based on the surrounding cationic sites. The relaxed O-Lu bond length of the five oxygen crystallographic sites are shown in Table S2 of the Supplementary Information. It is worthy to note that the bond length of one O_{21}-Lu1 bond is much longer than other cases of O-Lu bonds (including another O_{21}-Lu1 bond), indicating such Lu1 site is weakly bonded with O_{21}.

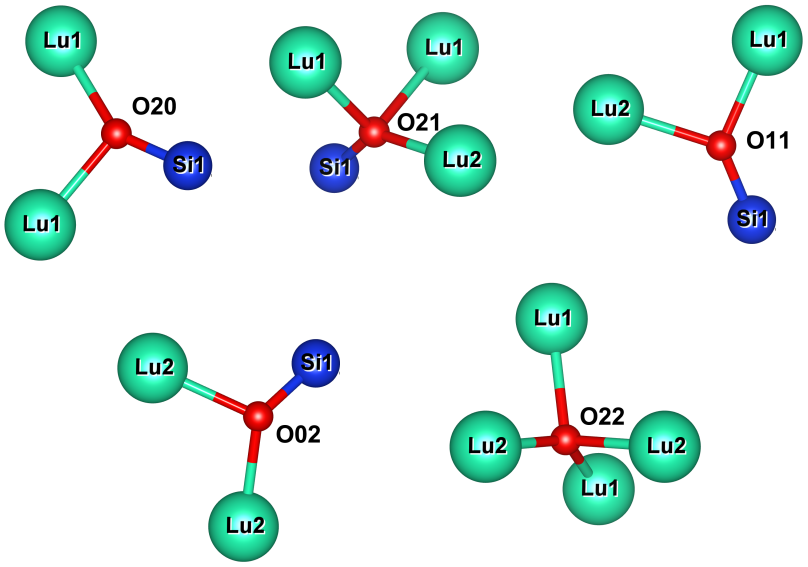

Figure 2: Oxygen sites in the crystal structure of Lu_2SiO_5.

Table 2: Coordination environment of the five different oxygen sites in Lu_2SiO_5 crystal. The label is inferred from the number of bonding Lu cations (digits from the Lu1 and Lu2 columns).

Oxygen Site	Lu1	Lu2	Si
O_{20}	2	0	1
O_{21}	2	1	1
O_{11}	1	1	1
O_{02}	0	2	1
O_{22}	2	2	0

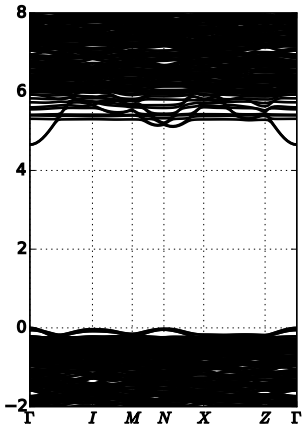

Figure 3: (Kohn-Sham) electron band structure of Lu_2SiO_5, conventional cell.

We computed the (Kohn-Sham) electronic band structure of the optimized bulk LSO conventional cell (Figure 3). The PBE-PAW band gap is 4.67 eV at the Γ point. This result is consistent with the reported PBE value,[38] but suffers from the well-known band gap problem of PBE, with sizable underestimation compared to experimental result, around 6.50 eV.[3] The charge densities of the HOMO and LUMO have been plot to check the composition of VBM and conduction band minimum (CBM), as shown in the Figure S1 of the Supplementary Information. The LSO results indicate that the VBM and CBM states are mainly composed by O_{2p} and Lu_{5d} state, respectively. The LDA band structures computed in the other three LDA+norm-conserving pseudopotential cases give results very similar in terms of the composition of VBM and CBM. These results are not shown here.

4. Oxygen vacancy stability in LSO

The existence of oxygen vacancies in LSO was first assumed based on the afterglow and TL behaviors of LSO:Ce scintillator, which maybe caused by the excited Ce_{5d} electron and/or Ce_{4f} hole being trapped in the oxygen vacancy. As

described in Sec 1, the current understanding of the stability of oxygen vacancies in the rare-earth orthosilicates with space group C2/c needs confirmation. In this section, we re-examine this issue in both LSO and YSO cases.

To study the relative stability of five kinds of oxygen vacancies as shown in Fig 2, detailed calculations have been conducted with different exchange-correlation functionals and the different pseudopotentials, for different supercells and charged states, as sketched previously.

To start with, we have observed that the formation energy of V_O^+ is higher than those of V_O and V_O^{2+}, except possibly in a very narrow range of permitted values of the Fermi level depending on the vacancy type. The PBE-PAW result, which is a typical case, is shown in the Figure S2 of the Supplementary Information. As a result, the formation energies of V_O^+ are not shown and neither discussed here, for clarity.

As mentioned in Sec.2.2, we have checked the convergence with respect to the supercell size. The Figure S3 of the Supplementary Information shows the typical formation energy of neutral and doubly positive charged oxygen vacancy in LSO from PBE-PAW pseudopotential case, using 127-atoms supercell. Compared to the result of Figure S2, it can be seen that the change of the formation energies of oxygen vacancy, using 63-atoms supercell, is less than 0.05 eV, and can hardly be seen on this figure. The Table S3 listed the detailed convergence study. The same convergence accuracy was also obtained for other LDA pseudopotential cases.

The conclusive results of the formation energy of oxygen vacancy in LSO are shown in Figure 4(a)-(d), for the PBE-PAW, LDA-FHI, LDA-Dojo and LDA-TM, respectively. The calculation with our LDA-TM pseudopotential gives a similar conclusion about oxygen vacancy stability, compared with the previous work on LSO[15]: they obtain that the most stable neutral and doubly positive charged oxygen vacancy is V_{O22}. However, this conclusion does not hold for the three other cases. At variance with the previous previous work and our LDA-TM calculation, the PBE-PAW, LDA-FHI and LDA-Dojo cases indicate that the most stable neutral oxygen vacancy in LSO forms at the oxygen sites within

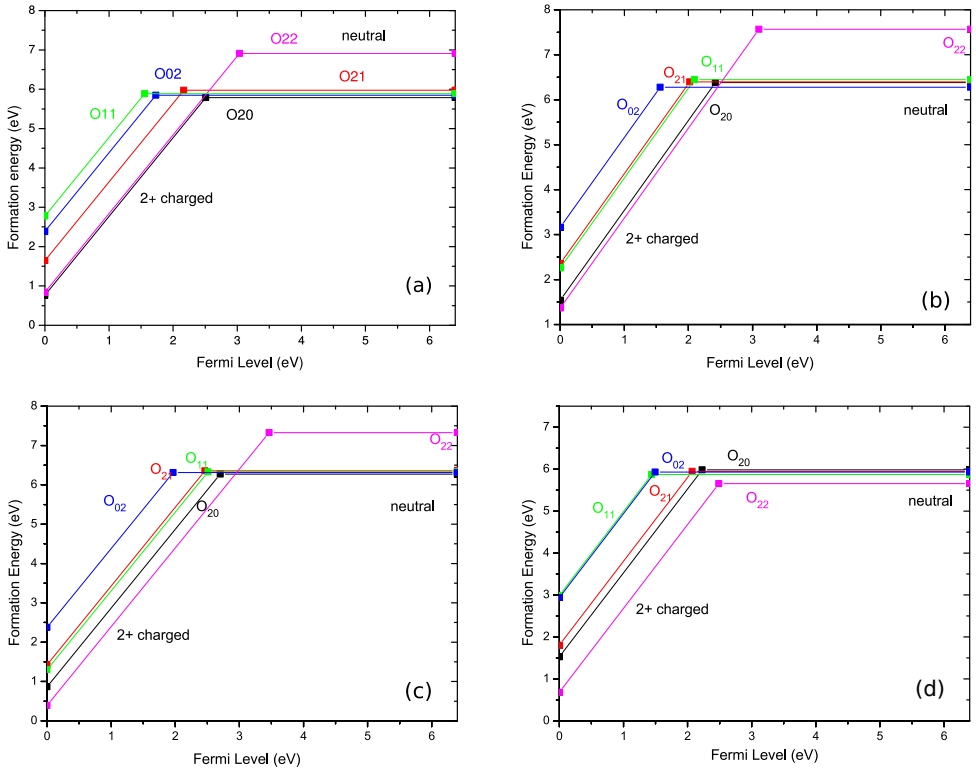

Figure 4: Formation energy of oxygen vacancy in Lu_2SiO_5: (a) PBE-PAW, (b) LDA-FHI, (c) LDA-Dojo and (d) LDA-TM.

the [SiO_4] tetrahedra. For the doubly positive charged case, the conclusion of old LDA-TM calculations agrees with our four cases. All results indicate that the most stable case is V_{O22}, which is consistent with the EPR measurement.[6]

We have performed similar calculations on the isostructural YSO compound. A similar difference was found between the results of LDA-TM and the other three cases. Figure S4 of the Supplementary Information shows the typical PBE-PAW result for the neutral and doubly positive charged oxygen vacancy stability in YSO. The result for the neutral case is consistent with the previous study about YSO[16], which indicates that the most stable neutral oxygen vacancy is from the oxygen site in [SiO_4] tetrahedra, but not from the oxygen vacancy that has no Si neighbor. This result is quite similar with the LSO one.

In the previous study of LSO[15], Liu *et al* proposed that the better stability of the neutral V_{O22} was due to the bigger bonding strength between Si-O than between Lu-O. Therefore, the energy needed to break the Si-O bond is larger than that of Lu-O. Such conclusion does not hold. As noticed by Zhou *et al* in the study of YSO,[16] the stability of oxygen vacancy should be related to bonding interaction between all the cation ions and oxygen, not only focusing on one single bonding energy. Indeed, from the viewpoint of bond dissociation energy, the bonding energy for Lu-O and Si-O equals 695 kJ/mol and 798 kJ/mol, respectively, and a simple bond dissociation counting due to the lower number of bonds gives the conclusion that the bond dissociation energies for V_{O20}, V_{O11} and V_{O02} are smaller than that of V_{O22}. However, this argument does not explain the energetic similarity of V_{O21} (three Lu neighbors) with V_{O20}, V_{O11} and V_{O02} (two Lu neighbors). The reason for the unexpected stability of V_{O21} might be due to the existence of the longest O-Lu (2.732 Å) in the coordinating environment of O_{21} site, as discussed in Section 3. Of course, the above discussion is crude since the bond counting model does not consider the effect of hybridization and different bond lengths.

Following this idea, we obtain a more accurate quantitative analysis of the bonding between the cations and oxygen in bulk LSO using the (projected) crystal orbital hamilton population (pCOHP) analysis as implemented in the LOBSTER code[31]. This method allows one to partition the entire band structure energy into pairwise inter-atomic interactions. The energy integral of the COHP qualitatively represents the strength of the bond. A positive pCOHP value indicates an anti-bonding interaction, and a negative pCOHP value indicates a bonding interaction. The result for LSO is shown in Fig 5. The curves in the upper section of Fig 5(a)-(e) indicate the total bonding interaction for the cation and oxygen in the five oxygen sites, and in the lower section Figs 5(f)-(j) show the partial contribution of each cation bonding with the oxygen atom. Fig 5 clearly shows that the four oxygen sites that are part of a Si-tetrahedron have similar bonding interaction, despite the differing number of Lu neighbors. The V_{O22} case is clearly different. These results are consistent with the forma-

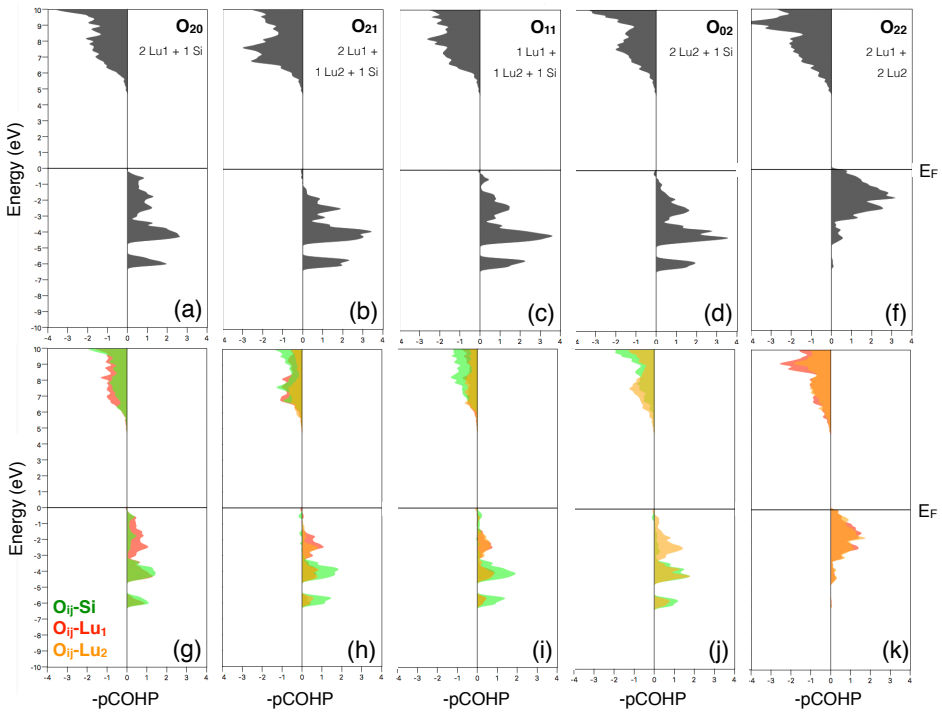

Figure 5: Total (upper row) and projected (lower row) crystal orbital Hamitonian populations (COHP) of the Si-O and Lu-O interations at the five oxygen sites, with PBE-PAW.

tion energy of neutral oxygen vacancy in LSO, as shown in Fig 4(a).

The agreement between PBE-PAW, LDA-FHI and LDA-Dojo cases leads us to believe that the LDA-TM case does not describe properly the oxygen vacancy formation. The LDA-TM pseudopotentials were generated a long time ago, and the quality of pseudopotentials has seen a noticeable improvement over the recent years, as described in Ref.[39].

5. The effect of Ce^{3+} ion doping

Cooke *et al* have studied the intrinsic trapping site in rare-earth oxyorthosilicates (Re_2SiO_5, Re = Y, Gd and Lu) [10, 11, 40]. They obtain that the TL behavior of rare earth oxyorthosilicates is not affected by the Ce^{3+} doping but

depends on the space group of the crystal structure. Indeed, the TL signals of YSO and LSO are quite similar, while they both differ from the one of Gd_2SiO_5 (space group P21/c).

In this section, we evaluate from first principles the effect of Ce^{3+} ion doping on the stability of oxygen vacancy in LSO. Before performing the study of LSO:Ce,V_O, calculations for LSO:Ce have been conducted. The DFT+U method successfully localizes the Ce_{4f} state inside the band gap. The total energies of LSO:Ce_{Lu1} and LSO:Ce_{Lu2} indicate that the Ce^{3+} ions prefer to enter the Lu1 site than Lu2 site, by lowering the energy of 45.93 kJ/mol. This preference of Ce^{3+} occupation might be due to the larger volume of the Lu1 coordination polyhedron than that of Lu2 site, which favors the larger Ce ion to occupy the looser site. Such assessment is consistent with the previous experimental and theoretical studies.[37, 41]

Table 3 lists the total energy and formation energy of neutral oxygen vacancy in LSO with and without Ce^{3+} ion doping. The total energy value of LSO bulk with 128-atom supercell is -73918.52 eV, which is not shown in Table 3. The effect of Ce^{3+} ion doping on the stability of oxygen vacancy can be evaluated from the difference of $\Delta E_{f,1}$ and $\Delta E_{f,2}$, where the $\Delta E_{f,1}$ and $\Delta E_{f,2}$ can be calculated as Eq.(2) and Eq.(3), respectively. The comparison between $\Delta E_{f,1}$ and $\Delta E_{f,2}$ is listed in the last column of Table 3. For most Ce^{3+} ion-doping cases, the effect on the stability of the oxygen vacancy is negligible, the energy difference being around 10 kJ/mol. Such energy difference can be matched by the single-crystal high temperature growth condition at 2150 °C,[42] related to energy change of around 20 kJ/mol (or 0.2 eV). However, it is worthy to note that the high temperature growth condition cannot change the relative stability of O_{22} with respect to the oxygen sites in [SiO_4] tetrahedral, with 100 KJ/mol (or 1.0 eV) formation energy difference.

Table 3: Formation energy of LSO:VO (,Ce) crystal, with 127-atom supercell. [Unit: eV]

case	E_{tot}(LSO:V_O)	$\Delta E_{f,1}$	Ce site	E_{tot}(LSO:Ce,V_O)	$\Delta E_{f,2}$	$\Delta E_{f,2}$ - $\Delta E_{f,1}$
V_{O20}	-73475.39	5.76	Lu1	-73394.51	5.66	-0.10
				-73394.45	5.71	-0.05
V_{O21}	-73475.21	5.95	Lu1	-73394.32	5.84	-0.09
			Lu1	-73394.12	6.04	0.09
			Lu2	-73393.95	5.75	-0.20
V_{O11}	-73475.30	5.83	Lu1	-73394.43	5.73	-0.10
			Lu2	-73394.04	5.67	-0.19
V_{O02}	-73475.33	5.83	Lu2	-73394.04	5.67	-0.19
				-73394.01	5.69	-0.13
V_{O22}	-73474.28	6.88	Lu1	-73393.31	6.86	-0.02
			Lu1	-73393.40	6.76	-0.10
			Lu2	-73392.93	6.77	-0.11
			Lu2	-73392.85	6.85	-0.03

6. Conclusion

We have studied the stability of neutral and charged oxygen vacancies in rare-earth oxyorthosilicate Lu_2SiO_5 with first principles calculations. The neutral oxygen vacancy in the [SiO_4] tetrahedral site has the lowest formation energy, while vacancies in the interstitial oxygen site bonded to lutetium atoms only are more difficult to form.

This contradicts results obtained one decade ago. We have tested different settings (exchange-correlation functionals and PAW or pseudopotentials) and observed that an old pseudopotential set favor the vacancy formation at the Lu-only bonded site, in contradiction with the results from more recent pseudopotentials, this being irrespective of the choice of exchange-correlation functional. This conclusion finds further support in the results of vacancy formation energy calculations in the isostructural compound Y_2SiO_5.

The higher formation energy of neutral oxygen vacancies in the interstitial

site compared to the other sites can be understood as coming from the bigger number of bonds to be broken (four Lu-O bonds), while in the other cases, a single Si-O and two Lu-O close bonds are broken. We also find that the incorporation of Ce^{3+} ion has a negligible effect on the stability of oxygen vacancy in the Lu-based oxyorthosilicate.

Acknowledgments

We acknowledge the help J.-M. Beuken for computational matters. This work, done in the framework of ETSF (project number 551), has been supported by the Fonds de la Recherche Scientifique (FRS-FNRS Belgium) through a Chargé de recherches fellowship (Y. Jia) and the PdR Grant No. T.0238.13 - AIXPHO (X. Gonze). Computational resources have been provided by the supercomputing facilities of the Université catholique de Louvain (CISM/UCL) and the Consortium des Equipements de Calcul Intensif en Fédération Wallonie Bruxelles (CECI) funded by the FRS-FNRS under Grant No. 2.5020.11.

References

[1] H. Suzuki, T. Tombrello, C. Melcher, J. Schweitzer, UV and gamma-ray excited luminescence of cerium-doped rare-earth oxyorthosilicates, Nucl. Instrum. Meth. Phys. Res., Sect. A. 320 (1992) 263–272.

[2] H. Suzuki, T. Tombrello, C. Melcher, J. Schweitzer, Light emission mechanism of Lu_2SiO_5: Ce, IEEE Trans. Nucl. Sci. 40 (1993) 380–383.

[3] U. R. Rodriguez-Mendoza, G. B. Cunningham, Y. Shen, K. L. Bray, High-pressure luminescence studies in $Ce^{3+} : Lu_2SiO_5$, Phys. Rev. B 64 (2001) 195112.

[4] L. Kappers, R. Bartram, D. Hamilton, A. Lempicki, J. Glodo, Thermal quenching and electron traps in LSO, J. Lumin. 102 (2003) 162–165.

[5] K. Yang, C. L. Melcher, P. D. Rack, L. A. Eriksson, Effects of calcium codoping on charge traps in LSO: Ce crystals, IEEE Trans. Nucl. Sci. 56 (2009) 2960–2965.

[6] V. V. Laguta, M. Buryi, J. Rosa, D. Savchenko, J. Hybler, M. Nikl, S. Zazubovich, T. Kärner, C. R. Stanek, K. J. McClellan, Electron and hole traps in yttrium orthosilicate single crystals: The critical role of Si-unbound oxygen, Phys. Rev. B 90 (2014) 064104.

[7] R. T. Shannon, C. T. Prewitt, Effective ionic radii in oxides and fluorides, Acta Crystallogr. B 25 (1969) 925–946.

[8] P. Dorenbos, C. W. E. v. Eijk, A. J. J. Bos, C. L. Melcher, Afterglow and thermoluminescence properties of Lu_2SiO_5: Ce scintillation crystals, J. Phys. Condens. Matter 6 (1994) 4167.

[9] J. D. Naud, T. A. Tombrello, C. L. Melcher, J. S. Schweitzer, The role of cerium sites in the scintillation mechanism of LSO, IEEE Trans. Nucl. Sci. 43 (1996) 1324–1328.

[10] D. W. Cooke, B. L. Bennett, R. E. Muenchausen, K. J. McClellan, J. M. Roper, M. T. Whittaker, Intrinsic trapping sites in rare-earth and yttrium oxyorthosilicates, J. Appl. Phys. 86 (1999) 5308–5310.

[11] D. W. Cooke, B. L. Bennett, K. J. McClellan, J. M. Roper, M. T. Whittaker, A. M. Portis, Electron-lattice coupling parameters and oscillator strengths of cerium-doped lutetium oxyorthosilicate, Phys. Rev. B 61 (2000) 11973–11978.

[12] L. Kappers, R. Bartram, D. Hamilton, A. Lempicki, J. Glodo, Thermal quenching and electron traps in LSO, J. Lumin 102 (2003) 162 – 165.

[13] Y. Yan, J. Karlsson, L. Rippe, A. Walther, D. Serrano, D. Lindgren, M.-e. Pistol, S. Kröll, P. Goldner, L. Zheng, J. Xu, Measurement of linewidths

and permanent electric dipole moment change of the $Ce\ 4f - 5d$ transition in Y_2SiO_5 for qubit readout scheme in rare-earth ion based quantum computing, Phys. Rev. B 87 (2013) 184205.

[14] J. D. Peak, C. L. Melcher, P. D. Rack, Investigating the luminescence properties as a function of activator concentration in single crystal cerium doped Lu_2SiO_5: Determination of the configuration coordinate model, J. Appl. Phys. 110 (2011) 013511.

[15] B. Liu, Z. Qi, M. Gu, X. Liu, S. Huang, C. Ni, First-principles study of oxygen vacancies in Lu_2SiO_5, J. Phys. Condens. Matter 19 (2007) 436215.

[16] B. Liu, J. Wang, F. Li, J. Wang, Y. Zhou, Mechanisms of mono-vacancy and oxygen permeability in Y_2SiO_5 orthosilicate studied by first-principles calculations, J. Am. Ceram. Soc. 95 (2012) 1093–1099.

[17] Y. D. Zavartsev, S. A. Koutovoi, A. I. Zagumennyi, Czochralski growth and characterisation of large $Ce^{3+} : Lu_2SiO_5$ single crystals co-doped with Mg^{2+} or Ca^{2+} or Tb^{3+} for scintillators, J. Cryst. Growth 275 (2005) e2167–e2171.

[18] M. A. Spurrier, P. Szupryczynski, K. Yang, A. A. Carey, C. L. Melcher, Effects of Ca^{2+} co-doping on the scintillation properties of LSO:Ce, IEEE Trans. Nucl. Sci. 55 (2008) 1178–1182.

[19] P. Blöchl, Projector augmented-wave method, Phys. Rev. B 50 (1994) 17953–17979.

[20] X. Gonze, B. Amadon, P.-M. Anglade, J.-M. Beuken, F. Bottin, P. Boulanger, F. Bruneval, D. Caliste, R. Caracas, M. Côté, T. Deutsch, L. Genovese, P. Ghosez, M. Giantomassi, S. Goedecker, D. Hamann, P. Hermet, F. Jollet, G. Jomard, S. Leroux, M. Mancini, S. Mazevet, M. Oliveira, G. Onida, Y. Pouillon, T. Rangel, G.-M. Rignanese, D. Sangalli, R. Shaltaf, M. Torrent, M. Verstraete, G. Zerah, J. Zwanziger,

ABINIT: First-principles approach to material and nanosystem properties, Comput. Phys. Commun. 180 (2009) 2582 – 2615.

[21] X. Gonze, F. Jollet, F. A. Araujo, D. Adams, B. Amadon, T. Applencourt, C. Audouze, J.-M. Beuken, J. Bieder, A. Bokhanchuk, E. Bousquet, F. Bruneval, D. Caliste, M. Côté, F. Dahm, F. D. Pieve, M. Delaveau, M. D. Gennaro, B. Dorado, C. Espejo, G. Geneste, L. Genovese, A. Gerossier, M. Giantomassi, Y. Gillet, D. Hamann, L. He, G. Jomard, J. L. Janssen, S. L. Roux, A. Levitt, A. Lherbier, F. Liu, I. Lukacevic, A. Martin, C. Martins, M. Oliveira, S. Poncé, Y. Pouillon, T. Rangel, G.-M. Rignanese, A. Romero, B. Rousseau, O. Rubel, A. Shukri, M. Stankovski, M. Torrent, M. V. Setten, B. V. troeye, M. Verstraete, D. Waroquier, J. Wiktor, B. Xue, A. Zhou, J. Zwanziger, Recent developments in the ABINIT software package, Comput. Phys. Commun. 205 (2016) 106.

[22] M. Torrent, F. Jollet, F. Bottin, G. Zérah, X. Gonze, Implementation of the projector augmented-wave method in the ABINIT code: Application to the study of iron under pressure, Comput. Mater. Sci. 42 (2008) 337 – 351.

[23] J. Perdew, K. Burke, M. Ernzerhof, Generalized gradient approximation made simple, Phys. Rev. Lett. 77 (1996) 3865–3868.

[24] F. Jollet, M. Torrent, N. Holzwarth, Generation of projector augmented-wave atomic data: A 71 element validated table in the XML format, Comput. Phys. Commun. 185 (2014) 1246 – 1254.

[25] N. Troullier, J. L. Martins, Efficient pseudopotentials for plane-wave calculations, Phys. Rev. B 43 (1991) 1993–2006.

[26] M. Fuchs, M. Scheffler, Ab initio pseudopotentials for electronic structure calculations of poly-atomic systems using density-functional theory, Comput. Phys. Commun. 119 (1999) 67 – 98.

[27] M. Van Setten, M. Giantomassi, E. Bousquet, M. J. Verstraete, D. R. Hamann, X. Gonze, G.-M. Rignanese, The pseudodojo: Training and grading a 85 element optimized norm-conserving pseudopotential table, Comput. Phys. Commun. 226 (2018) 39–54.

[28] G. Petretto, X. Gonze, G. Hautier, G.-M. Rignanese, Convergence and pitfalls of density functional perturbation theory phonons calculations from a high-throughput perspective, Comput. Mater. Sci. 144 (2018) 331.

[29] Y. Jia, S. Poncé, A. Miglio, M. Mikami, X. Gonze, Assessment of first-principles and semiempirical methodologies for absorption and emission energies of Ce^{3+}-doped luminescent materials, Adv. Opt. Mater. 5 (2017) 1600997.

[30] N. Holzwarth, A. Tackett, G. Matthews, A projector augmented wave (PAW) code for electronic structure calculations, part I: ATOMPAW for generating atom-centered functions, Comput. Phys. Commun. 135 (2001) 329 – 347.

[31] V. L. Deringer, A. L. Tchougréeff, R. Dronskowski, Crystal orbital Hamilton population (COHP) analysis as projected from plane-wave basis sets, J. Phys. Chem. A 115 (2011) 5461–5466.

[32] R. Dronskowski, P. E. Bloechl, Crystal orbital hamilton populations (COHP): energy-resolved visualization of chemical bonding in solids based on density-functional calculations, J. Phys. Chem. 97 (1993) 8617–8624.

[33] A. Miglio, C. P. Heinrich, W. Tremel, G. Hautier, W. G. Zeier, Local bonding influence on the band edge and band gap formation in quaternary chalcopyrites, Adv. Sci. 4 (2017) 1700080.

[34] C. Freysoldt, B. Grabowski, T. Hickel, J. Neugebauer, G. Kresse, A. Janotti, C. G. Van de Walle, First-principles calculations for point defects in solids, Rev. Mod. Phys. 86 (2014) 253–305.

[35] C. Freysoldt, J. Neugebauer, C. G. Van de Walle, Fully ab initio finite-size corrections for charged-defect supercell calculations, Phys. Rev. Lett. 102 (2009) 016402.

[36] R. D. Shannon, Dielectric polarizabilities of ions in oxides and fluorides, J. Appl. Phys. 73 (1993) 348–366.

[37] L. Pidol, O. Guillot-Nol, A. Kahn-Harari, B. Viana, D. Pelenc, D. Gourier, EPR study of Ce^{3+} ions in lutetium silicate scintillators $Lu_2Si_2O_7$ and Lu_2SiO_5, J. Phys. Chem. Solids 67 (2006) 643–650.

[38] L. Ning, L. Lin, L. Li, C. Wu, C.-k. Duan, Y. Zhang, L. Seijo, Electronic properties and 4f $\rightarrow$ 5d transitions in Ce-doped Lu_2SiO_5: a theoretical investigation, J. Mater. Chem. 22 (2012) 13723–13731.

[39] K. Lejaeghere, G. Bihlmayer, T. Björkman, P. Blaha, S. Blügel, V. Blum, D. Caliste, I. E. Castelli, S. J. Clark, A. D. Corso, S. de Gironcoli, T. Deutsch, J. K. Dewhurst, I. D. Marco, C. Draxl, M. Dułak, O. Eriksson, J. A. Flores-Livas, K. F. Garrity, L. Genovese, P. Giannozzi, M. Giantomassi, S. Goedecker, X. Gonze, O. Grånäs, E. K. U. Gross, A. Gulans, F. Gygi, D. R. Hamann, P. J. Hasnip, N. A. W. Holzwarth, D. Iusan, D. B. Jochym, F. Jollet, D. Jones, G. Kresse, K. Koepernik, E. Küçükbenli, Y. O. Kvashnin, I. L. M. Locht, S. Lubeck, M. Marsman, N. Marzari, U. Nitzsche, L. Nordström, T. Ozaki, L. Paulatto, C. J. Pickard, W. Poelmans, M. I. J. Probert, K. Refson, M. Richter, G.-M. Rignanese, S. Saha, M. Scheffler, M. Schlipf, K. Schwarz, S. Sharma, F. Tavazza, P. Thunström, A. Tkatchenko, M. Torrent, D. Vanderbilt, M. J. van Setten, V. V. Speybroeck, J. M. Wills, J. R. Yates, G.-X. Zhang, S. Cottenier, Reproducibility of density functional theory calculations of solids, Science 351 (2016) aad3000.

[40] D. W. Cooke, B. L. Bennett, K. J. McClellan, J. M. Roper, M. T. Whittaker, Similarities in glow peak positions and kinetics parameters of oxy-

orthosilicates: evidence for unique intrinsic trapping sites, J. Lumin. 92 (2000) 83–89.

[41] A. Y. Kuznetsov, A. B. Sobolev, A. N. Varaksin, O. A. Keda, Embedded cluster calculations of the electron structure of the Ce^{3+} impurity in Lu_2SiO_5 crystals with allowance for crystal lattice relaxation and polarization, Phys. Status Solidi B 204 (1997) 701–712.

[42] A. Yoshikawa, V. Chani, M. Nikl, Czochralski growth and properties of scintillating crystals, Acta Phys. Pol. A 124 (2013) 251.